

Supporting Online Information

Electroluminescence in Aligned Arrays of Single-Wall Carbon Nanotubes with Asymmetric Contacts

Xu Xie,^{†,‡} Ahmad E. Islam,^{†,‡} Muhammad A. Wahab,^{#,‡} Lina Ye,^{†,§} Xinning Ho,^{†,⊥} Muhammad A. Alam,^{#,} and John A. Rogers^{†,||,*}*

[†]Department of Materials Science and Engineering and Frederick Seitz Materials Research Laboratory, University of Illinois, Urbana, Illinois 61801, United States.

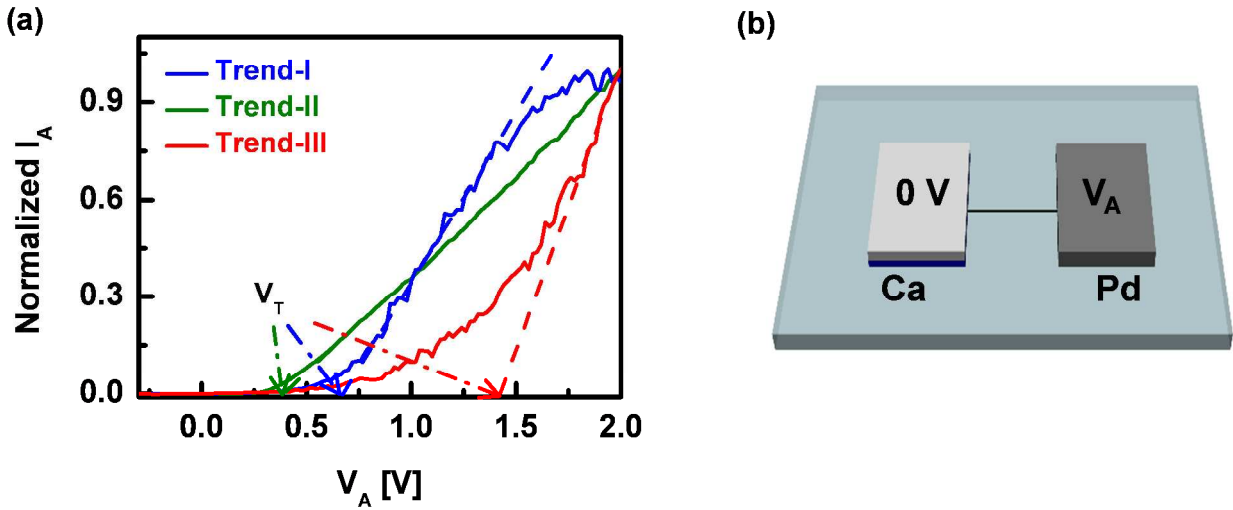
[#]School of Electrical and Computer Engineering, Purdue University, West Lafayette, Indiana 47907, United States.

^{||}Departments of Chemistry, Mechanical Science and Engineering, Electrical and Computer Engineering, Beckman Institute for Advanced Science and Technology, University of Illinois, Urbana, Illinois 61801, United States.

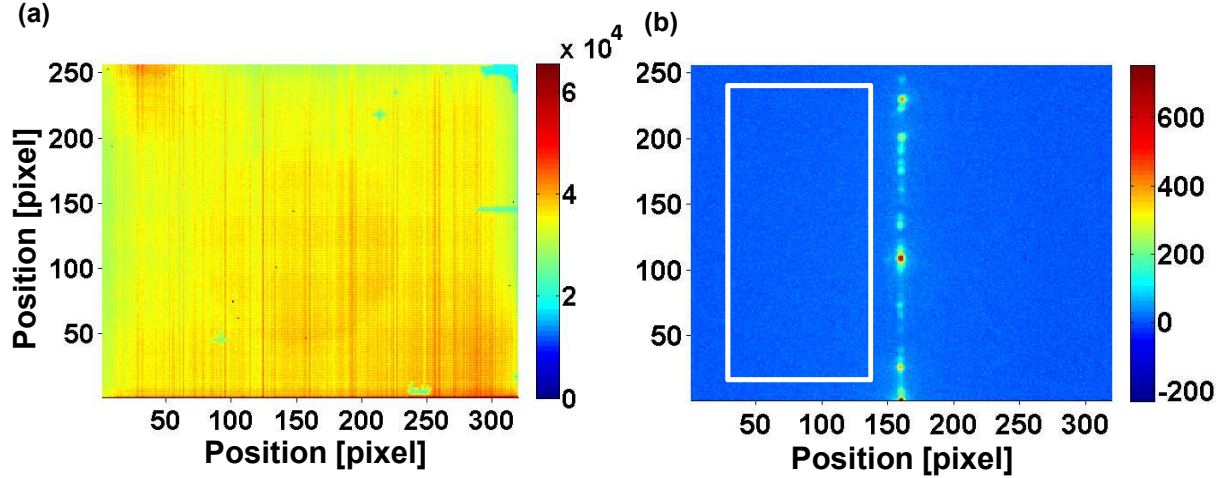
[§] Present address: Department of Chemistry, Anhui University, Hefei 230039, China.

[⊥] Present address: Singapore Institute of Manufacturing Technology, Singapore 638075.

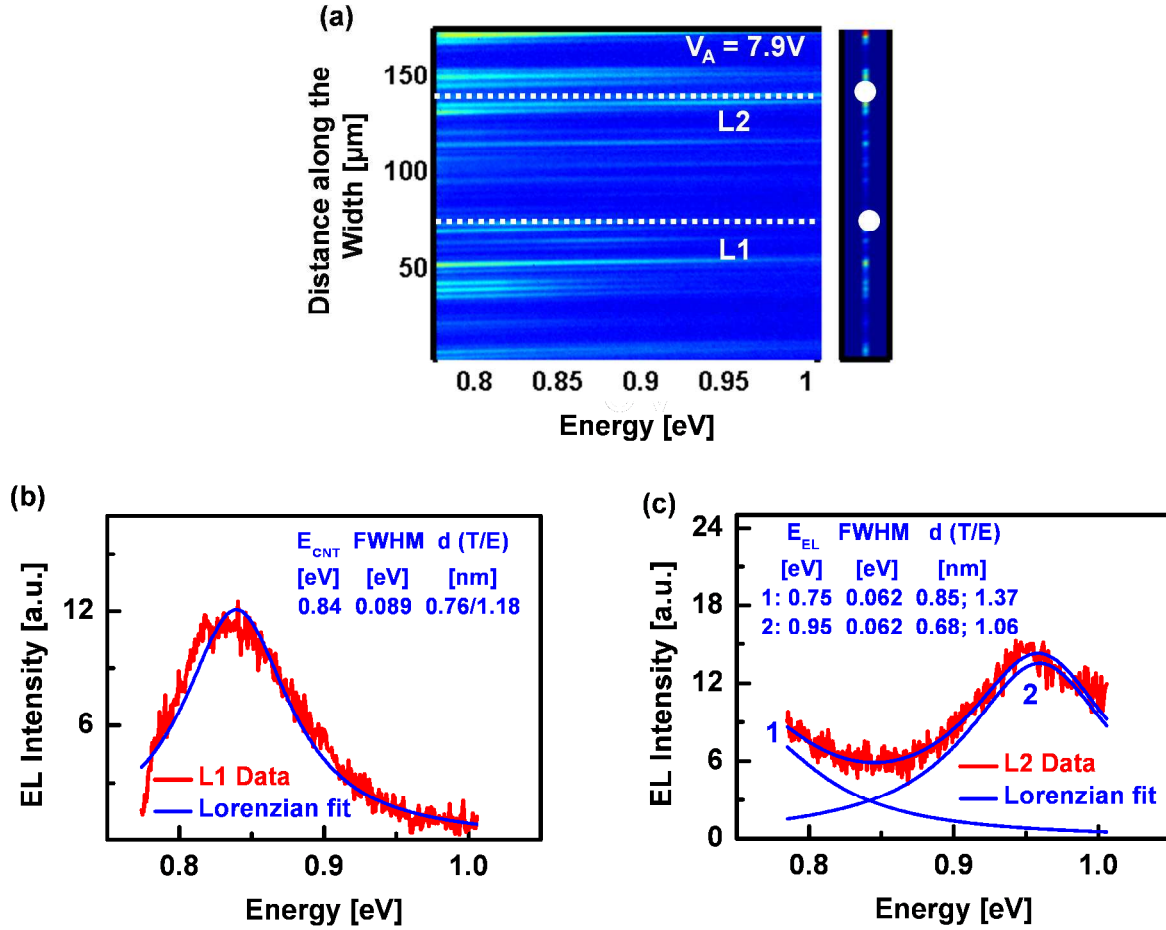
[‡]These authors contributed equally.



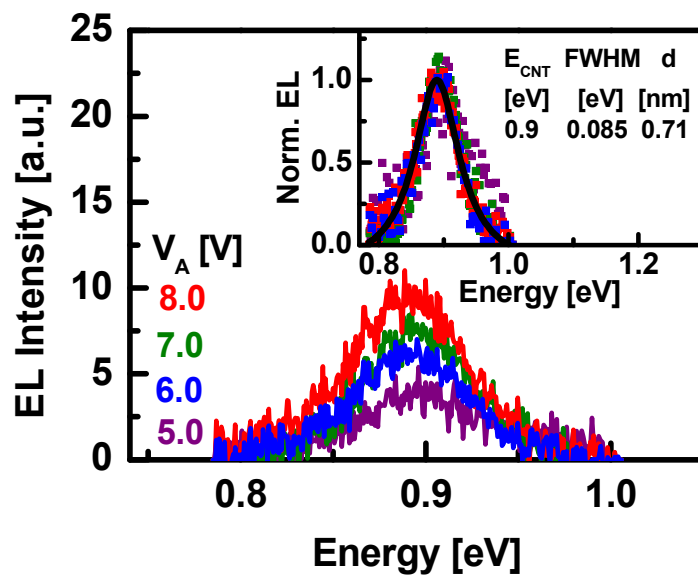
Supporting Figure 1. (a) Normalized I_A (with respect to maximum I_A) vs. V_A for three representative devices that each incorporate a single s-SWNT with Ca and Pd contacts. (b) Schematic illustration of the devices. Of the thirty such devices that were studied, eleven showed non-linear behavior in I_A vs. V_A near the threshold (V_T), linearity above V_T and saturation at $V_A \gg V_T$ (trend-I); nine devices showed no saturation at higher V_A (trend-II); the remaining ten devices predominantly show non-linear behavior near V_T (trend-III). In all cases, V_T is calculated from the x-axis intercept of a line fitted to the linear region of behavior.



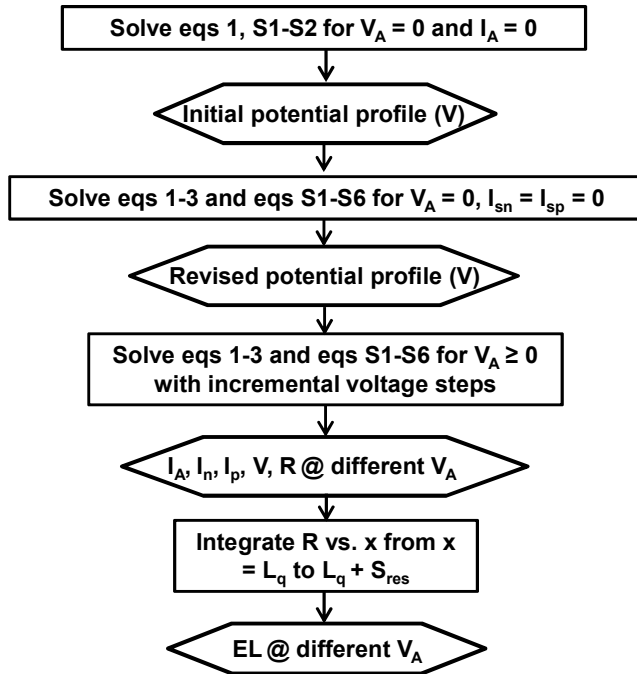
Supporting Figure 2. (a) Dark signal (average ~ 36000 counts/pixel for 15 s integration time) measured by using the experimental setup with zero bias on the 2T-LEDs (*i.e.*, for $V_A = 0$ V). With this level of dark signal, the maximum detected signal of CCD camera is, $N_{\text{signal}} = (2^{16} - 36000) \sim 29,536$ counts/pixel. The resultant dark noise and shot noise levels are, $N_{\text{dark}} = \sqrt{36000} \sim 189.7$ counts/pixel and $N_{\text{shot}} = \sqrt{29536} \sim 171.9$ counts/pixel. Considering read-out noise $N_{\text{readout}} = 500$ counts/s,¹ we calculate total noise of $N_{\text{total}} = \sqrt{(N_{\text{shot}}^2 + N_{\text{dark}}^2 + N_{\text{readout}}^2)} \sim 256$ counts/pixel in our imaging system. (b) This value of N_{total} is consistent with the measured noise level of $\sim 113 \pm 123$ counts/pixel (for 15 s integration time) within the white boundary.



Supporting Figure 3. (a) Plot of EL spectra measured along the width of a device (*i.e.*, perpendicular to the alignment direction of SWNT arrays) near the Ca contact. The frame on the right shows the spatial profile of the integrated EL. The white dots correspond to the dashed white lines on the left. EL spectra collected at spots L1 and L2 appear in (b) and (c) respectively. These spectra can be fitted by considering contributions from one or two s-SWNTs that may be present within scan resolution ($S_{res} \sim 1.5 \mu m$)² of the camera/spectrometer setup. Lorentzian lineshapes with FWHM $\sim 0.06\text{--}0.09$ were used, with emission peaks (E_{CNT}) and corresponding diameters (d) shown in the insets. $E_{CNT} = E_g - E_{binding}$ is used to estimate diameter both theoretically³⁻⁵(T) and empirically⁶(E).



Supporting Figure 4. EL spectra collected at a particular spot near the Ca contact of a 2T-LED for different V_A . The inset show normalized data, which suggest negligible change of emission profiles with V_A . Spectra at any V_A can be fitted using a Lorentzian function with peak at $E_{CNT} \sim 0.9$ eV and FWHM ~ 0.085 eV. Using theoretical ($E_{CNT} = 0.84/d - E_{binding}$)³⁻⁵ and empirical ($E_{CNT} \sim 1.11/(d + 0.11)$)⁶ expressions, peak at 0.9 eV corresponds to EL from s-SWNT with $d \sim 0.71/1.12$ nm (theoretical/empirical, T/E).



Supporting Figure 5. Flowchart to simulate current transport and electroluminescence (EL) in 2T-LEDs. See Supporting Information Section 1 for related equations and definition of variables.

Supporting Section 1: Simulation Steps

Simulation of a 2T-LED containing a single s-SWNT with particular diameter (d) involves self-consistent solution of electrostatics and current flow. We solve electrostatics (using eq 1 of the main text) with Dirichlet boundary conditions at Ca and Pd contacts (*i.e.*, potentials at Ca and Pd contacts equal $-\Phi_{Ca}$ and $V_A - \Phi_{Pd}$, where $\Phi_{Ca(Pd)}$ is work-function difference between Ca (Pd) and s-SWNT) and Von-Neumann boundary conditions (*i.e.*, zero electric field) along the exposed surface of the dielectric.⁷ Detailed expressions for electron and hole concentrations (n and p) and ionized impurity (N_a^-) as used in eq 1 are given below:

$$n(p) = N_C \mathfrak{F}_{1/2}(\eta_{n(p)}) \quad \text{--- (S1)}$$

$$N_a^- = N_a / \left[1 + 4 \exp \left[(E_V - E_{Fp} + 0.045) / k_B T \right] \right] \quad \text{--- (S2)}$$

where $N_C = \frac{8\alpha}{a} \left(\frac{E_g + k_B T}{E_g + 4\gamma_0} \right) \sqrt{\frac{k_B T}{3\pi E_g}}$ is the effective density of states,⁸

$\eta_n = \frac{E_{Fn} - E_C}{k_B T}$, $\eta_p = \frac{E_V - E_{Fp}}{k_B T}$, $\mathfrak{F}_{1/2}$ is the Fermi-Dirac integral of order $1/2$, $\alpha = 1-2$ is the zone degeneracy factor, $a = 0.246$ nm is the graphene Bravais lattice constant, $E_g \sim 0.84/d$ (in nm) is the bandgap of s-SWNT, $\gamma_0 \sim 3$ eV is the nearest neighbor overlap energy, $E_{C(V)}$ is the conduction (valence) band energies, and $E_{Fn(p)}$ is quasi-Fermi level for electrons (holes). Ionized impurity with $N_a = 5 \times 10^{19} \text{ cm}^{-3}$ is used to capture the influence of negatively charged interface defect⁹ on the electrostatics of s-SWNT.

We calculate currents in 2T-LED using the drift-diffusion equations (eqs 2-3 of the main text). Detailed expressions for mobility (μ_{FE}), diffusion co-efficients for electron and hole ($D_{n(p)}$), and $G_{SBT,n(p)}$ as used in eqs 2-3 are given below:

$$\mu_{FE} = \frac{\mu_{peak}}{1 + \mu_{peak} \left| \frac{dV}{dx} \right| / v_s} \quad \text{---(S3)}$$

$$D_{n(p)} = \left(\frac{k_B T}{q} \mu_{FE, n(p)} \right) \mathfrak{F}_{1/2}(\eta_{n(p)}) / \mathfrak{F}_{-1/2}(\eta_{n(p)}) \quad \text{---(S4)}$$

$$G_{SBT, n(p)} = \frac{\pi \left| \frac{dV}{dx} \right| A T a d}{k_B} \left[\begin{array}{l} \exp \left[-\frac{2\sqrt{2m}}{\hbar} \int_0^x \sqrt{E_{rx, C(V)}} dr \right] \ln \left[\frac{1 + \exp \eta_{n(p)}}{1 + \exp \eta_{n(p), Ca}} \right] + \\ \exp \left[-\frac{2\sqrt{2m}}{\hbar} \int_x^L \sqrt{E_{rx, C(V)}} dr \right] \ln \left[\frac{1 + \exp \eta_{n(p)}}{1 + \exp \eta_{n(p), Pd}} \right] \end{array} \right] \quad \text{---(S5)}$$

where $\mu_{peak} = 1600 \left(\frac{300}{T} \right) \left(\frac{d}{1nm} \right)^2$,¹⁰ v_s is the saturation velocity, $\eta_{n, Ca(Pd)} = (E_{F, Ca(Pd)} - E_C) / k_B T$, $\eta_{p, Ca(Pd)} = (E_V - E_{F, Ca(Pd)}) / k_B T$, $E_{rx, C} = E_C(r) - E_C(x)$, $E_{rx, V} = E_V(x) - E_V(r)$, $m = \frac{E_g}{20} m_0$ is the effective mass for electrons and holes, m_0 is the free carrier effective mass, \hbar is the reduced Planck's constant, $E_{F, Ca(Pd)}$ is the Fermi-level for carriers in Ca (Pd) contact, $A = 1.5 \times 10^2 E_g$ A/cm²/K² is the Richardson constant, and a is the thickness of s-SWNT.

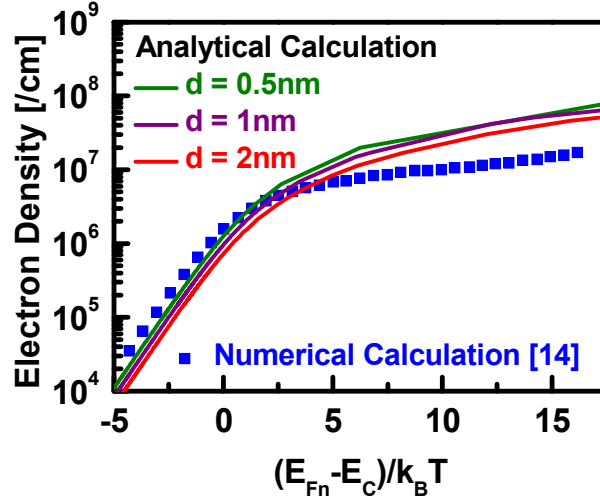
As explained in Supporting Information Figure 5, we start 2T-LED simulation by solving eq 1 (main text) and eqs S1-S2 in equilibrium (*i.e.*, at $V_A = 0$ and $I_A = 0$), and then revise the calculated potential V by solving eqs 1-3 (main text) and eqs S3-S5 with zero electron and hole boundary currents (I_{sn} and I_{sp}) that have the following expressions:

$$I_{sn} = qv_{sn} (n|_{Ca, Pd} - n_{equi}); I_{sp} = qv_{sp} (p|_{Ca, Pd} - p_{equi}) \quad \text{--- (S6)}$$

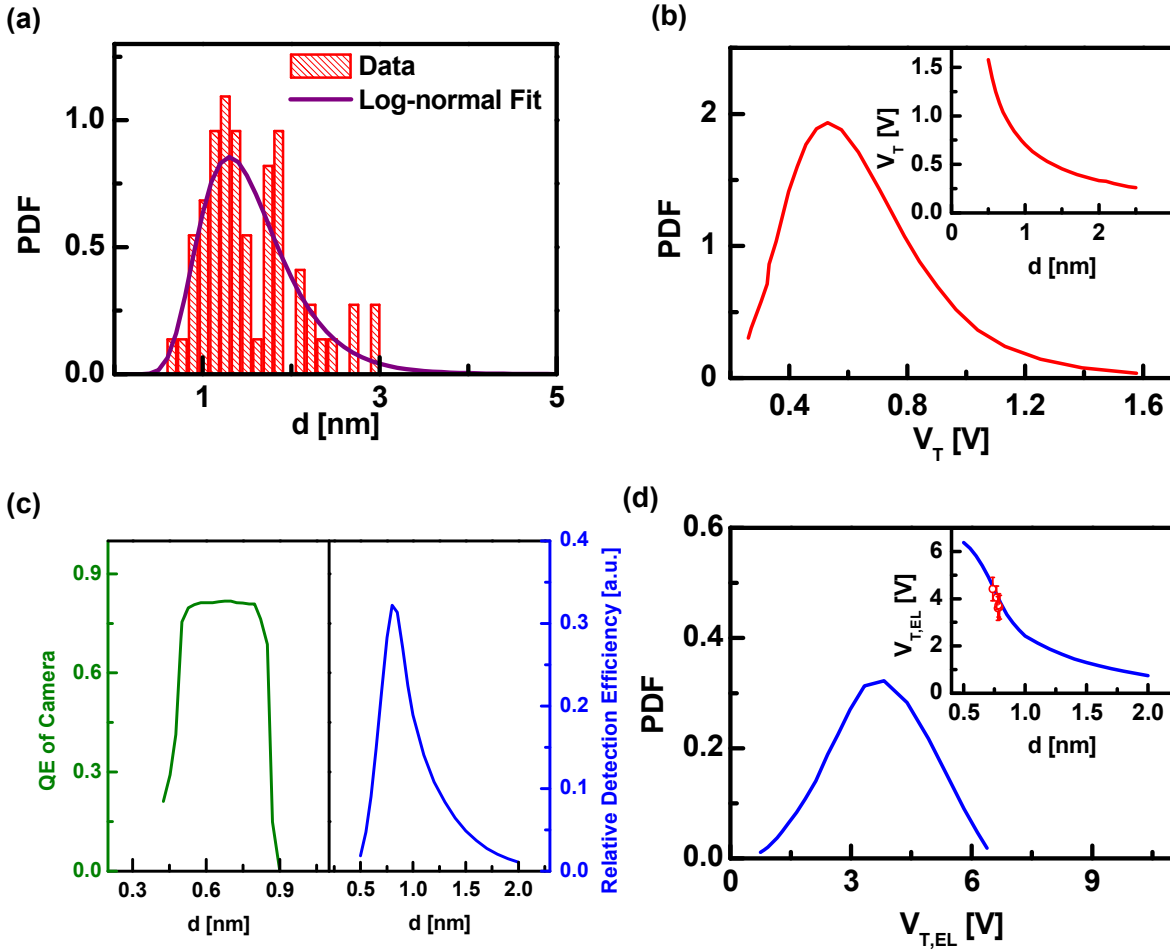
where $n(p)|_{Ca, Pd}$ is the electron (hole) concentrations at the Ca/SWNT and Pd/SWNT interfaces and is obtained by solving eqs 2-3 (main text), $n_{equi} = N_C \mathfrak{F}_{1/2}(\eta_{n, Ca} \text{ or } \eta_{n, Pd})$,

$p_{equi} = N_C \mathfrak{F}_{1/2}(\eta_{p,Ca} \text{ or } \eta_{p,Pd})$, $v_{sn(sp)}$ is the surface recombination velocity of electron (hole) and equals half of the thermal velocity.¹¹

Equilibrium solution of n, p, V, E_C, E_V is later used to solve eqs 1-3 (main text) and eqs S1-S6 in non-equilibrium ($V_A \geq 0, I_A = I_n + I_p \neq 0$) conditions with incremental voltage steps for V_A . Such solution also provides R (*i.e.*, EHR rate) vs. x , which is used to estimate EL intensity by integrating R from L_q to $L_q + S_{res}$ (since EHR within $x = 0 \sim L_q$ is quenched), where L_q is the exciton quenching length and S_{res} is the spatial resolution of the IR camera. To directly compare the calculated EL intensity with measured values, we need to take into account the quantum efficiency of EL in s-SWNT that ranges from 10^{-4} - 10^{-9} .^{2,12,13}

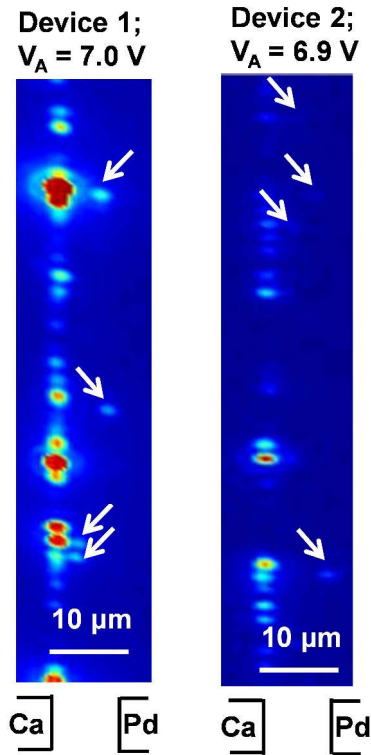


Supporting Figure 6. Plot of calculated electron density vs. relative change of Fermi level (E_{Fn}) with respect to the conduction band (E_C) of s-SWNTs for different diameters (indicated in the legend) follow a universal trend.¹⁴ Though analytical equations over-estimate electron density-of-states at degenerate energy levels (*i.e.*, for $E_{Fn} \gg E_C$) and hence calculate larger electron density compared to detailed numerical calculations,¹⁴ we use analytical approaches for rapid simulation.



Supporting Figure 7. (a) Measured SWNT diameter distribution¹⁵ (PDF: probability distribution function) and fitted curve based on log-normal statistics. (b) Plot of simulated distribution in V_T , calculated using the diameter distribution and relationship between V_T vs. d (inset). (c) Quantum efficiency (QE) of the InGaAs camera (green line) limits the diameter distribution for s-SWNTs that give rise to detectable EL. Calculated relative detection efficiency (blue line) considering Lorentzian distributions (FWHM ~ 0.1 eV) for EL responses from individual s-SWNTs and a diameter independence for the EL intensity, suggests that the camera will mainly detect EL for $d \sim 0.5$ - 2.0 nm s-SWNTs. (d) Plot of simulated distribution in $V_{T,EL}$, as calculated using the relative detection efficiency and the relationship between $V_{T,EL}$ vs. d (inset). The simulated $V_{T,EL}$ vs. d relationship was calibrated with the measured values, as obtained from

a few spots of Figure 4a. The diameter range ($d \sim 0.63\text{-}0.82$ nm) for these measured values obtained using theoretical approaches³⁻⁵ is limited by the detectable wavelength range ($\lambda = 1200\text{-}1600$ nm). (Consideration of any dependence of EL intensity on d at a particular V_A (Figure 6b) will change the calculated distribution of $V_{T,EL}$. To calculate QE vs. d , we use QE vs. λ ¹ and calculate d using theoretical approaches,³⁻⁵ *i.e.*, using $0.84/(hc/\lambda - E_{\text{binding}})$, where h is Planck's constant, c is the velocity of light, and E_{binding} is the binding energy for exciton dissociation.)



Supporting Figure 8. In addition to EL near the Ca contacts, at high voltages, EL appears at other positions (arrows), possible due to large local values of E_{field} (hot spots) due to defects.¹⁶

REFERENCES FOR SUPPORTING MATERIALS

1. <http://www.roperscientific.de/datasheets/CCD%20detection%20limits.pdf>.
2. Zaumseil, J.; Ho, X. N.; Guest, J. R.; Wiederrecht, G. P.; Rogers, J. A. Electroluminescence from Electrolyte-Gated Carbon Nanotube Field-Effect Transistors. *ACS Nano* **2009**, *3*, 2225-2234.
3. Saito, R.; Dresselhaus, G.; Dresselhaus, M. S. Physical Properties of Carbon Nanotubes. Imperial College Press: London, 1998.
4. Liao, A.; Zhao, Y.; Pop, E. Avalanche-Induced Current Enhancement in Semiconducting Carbon Nanotubes. *Phys. Rev. Lett.* **2008**, *101*, 256804.
5. Perebeinos, V.; Tersoff, J.; Avouris, P. Scaling of Excitons in Carbon Nanotubes. *Phys. Rev. Lett.* **2004**, *92*, 257402.
6. Dukovic, G.; Wang, F.; Song, D. H.; Sfeir, M. Y.; Heinz, T. F.; Brus, L. E. Structural Dependence of Excitonic Optical Transitions and Band-Gap Energies in Carbon Nanotubes. *Nano Lett.* **2005**, *5*, 2314-2318.
7. Guo, J. Carbon Nanotube Electronics: Modeling, Physics, and Applications. Ph.D. Dissertation, Purdue University, West Lafayette, **2004**.
8. Akinwande, D.; Nishi, Y.; Wong, H. S. P. An Analytical Derivation of the Density of States, Effective Mass, and Carrier Density for Achiral Carbon Nanotubes. *IEEE Trans. Electron Devices* **2008**, *55*, 289-297.
9. Kim, W.; Javey, A.; Vermesh, O.; Wang, O.; Li, Y. M.; Dai, H. J. Hysteresis Caused by Water Molecules in Carbon Nanotube Field-Effect Transistors. *Nano Lett.* **2003**, *3*, 193-198.
10. Perebeinos, V.; Tersoff, J.; Avouris, P. Electron-Phonon Interaction and Transport in Semiconducting Carbon Nanotubes. *Phys. Rev. Lett.* **2005**, *94*, 086802.

11. Traversa, F. L.; Bertazzi, F.; Bonani, F.; Guerrieri, S. D.; Ghione, G.; Perez, S.; Mateos, J.; Gonzalez, T. A Generalized Drift-Diffusion Model for Rectifying Schottky Contact Simulation. *IEEE Trans. Electron Devices* **2010**, *57*, 1539-1547.
12. Mueller, T.; Kinoshita, M.; Steiner, M.; Perebeinos, V.; Bol, A. A.; Farmer, D. B.; Avouris, P. Efficient Narrow-Band Light Emission from a Single Carbon Nanotube P-N Diode. *Nature Nanotechnology* **2010**, *5*, 27-31.
13. Wang, S.; Zeng, Q. S.; Yang, L. J.; Zhang, Z. Y.; Wang, Z. X.; Pei, T. A.; Ding, L.; Liang, X. L.; Gao, M.; Li, Y., *et al.* High-Performance Carbon Nanotube Light-Emitting Diodes with Asymmetric Contacts. *Nano Lett.* **2011**, *11*, 23-29.
14. Liang, J.; Akinwande, D.; Wong, H. S. P. Carrier Density and Quantum Capacitance for Semiconducting Carbon Nanotubes. *J. Appl. Phys.* **2008**, *104*, 064515.
15. Islam, A. E.; Du, F.; Ho, X.; Jin, S. H.; Dunham, S.; Rogers, J. A. Effect of Variations in Diameter and Density on the Statistics of Aligned Array Carbon-Nanotube Field Effect Transistors. *J. Appl. Phys.* **2012**, *111*, 054511.
16. Freitag, M.; Johnson, A. T.; Kalinin, S. V.; Bonnell, D. A. Role of Single Defects in Electronic Transport Through Carbon Nanotube Field-Effect Transistors. *Phys. Rev. Lett.* **2002**, *89*, 216801.